5th Canadian Conf. Earthquake Engineering / Ottawa / 1987 / 5ème Conf. Canadienne Génie Sismique

Dynamic behavior of prestressed egg-shaped tanks during strong ground motions

F.Miura & S.Hamada
Yamaguchi University, Tokiwadai, Japan

H.Nakamura
Mazda Motor Corporation, Japan

S.Morikawa
Asano Engineering Co. Ltd, Japan

ABSTRACT: The purpose of this paper is to investigate the dynamic behavior of egg-shaped tanks with different foundations. The axi-symmetric finite element technique is adopted in the analysis. A viscous boundary formulation is also established for this problem instead of using the infinite boundary of the ground.

1 INTRODUCTION

Egg-shaped prestressed concrete tanks have been developed as the structure of sludge treatment. These tanks have several advantages in digesting functions, mechanical equipments and maintenance. The tanks are recently introduced into Japan which is subjected to frequent earthquakes. In such an earthquake-prone country, the structures requires rational aseismic design so as to resist strong earthquake motions. Research and design codes on the egg-shaped concrete tank under seismic loads are still limited (Yoshida et al. 1984, Nagasawa et al. 1983).

Present study aims to provide design information for egg-shaped prestressed concrete tanks under seismic loading. The axi-symmetric finite element technique is employed in the analysis of water-soil-structure interaction under the condition of an non-symmetric loading. To obtain dynamic response of soil-tank interaction system, energy absorption at the artificial boundary need to be included in the analysis. In order to absorb the radiation wave energy on the boundary a viscous boundary has been employed in 2-dimensional problems by several researchers (Lysmer et al. 1969, Lysmer et al. 1975).

A viscous boundary formulation is newly developed for axi-symmetric system subjected to non-symmetric loads in this study. With aid of the present proposed viscous boundary technique, dynamic stresses produced in the tank wall and the base ring are evaluated under dynamic excitation obtained from the past earthquake. Behavioral studies related to foundation is also conducted. The maximum accelerations, displacements and dynamic stresses are obtained and discussed for four models of foundation, that is, direct ring, footing and pile foundations.

2 EQUATION OF MOTION

2.1 Principle of virtual work

Based on the principle of virtual work, the following equation is applied to the dynamic problem.

$$\int_V \delta\{\varepsilon\}^T\{\sigma\}\,dV - \int_V \delta\{u\}^T(\{F\} - \eta\{\dot{u}\} - \rho\{\ddot{u}\})\,dV - \int_S d\{u\}^T\{T\}\,dS = 0 \qquad (1)$$

where $\{\varepsilon\}$ is a virtual strain vector, and $\{\sigma\}$, $\{F\}$, $\{u\}$, and $\{T\}$ are stress, body force, displacement and traction vectors, respectively. The suffix, T, and dot, $\cdot$, imply transverse and derivative with respect to time, respectively. Coefficients η and ρ are the cohesive coefficient and density, respectively.

The equation of motion in a system having free side boundaries and a sufficiently rigid base is obtained as the following matrix equation. This equation is obtained by letting $\{F\}=0$ and $\int_S d\{u\}^T\{T\}\,dS = 0$.

$$[M]\{\ddot{\delta}\} + [C]\{\dot{\delta}\} + [K]\{\delta\} = -[M]\{I\}\ddot{u}_g \qquad (2)$$

where [M], [C] and [K] are mass, damping and stiffness matrices, respectively. $\{\delta\}$ and $\{I\}$ are the nodal displacement and

unit vectors, respectively. u_g represents the input displacements on the basal layer.

To obtain the viscous boundary formulation, the 3rd term of Eq.(1) must be determined. This term includes the virtual works done by (1) radiation wave to the basal layer, (2) radiation wave to the free field and (3) motion of the free field. Fig.1 illustrates the typical soil-structure interaction system surrounded by the basal layer and free field. The equation of motion can be obtained by adding the terms obtained from these virtual works to Eq.(2), which is given by (Miura et al. 1986)

$$
\begin{aligned}
&[M]\{\ddot{\delta}\}+[C]\{\dot{\delta}\}+[K]\{\delta\}\\
&+[C_B]\{\dot{\delta}_B\}+[C_s](\{\dot{\delta}_s\}-\{\dot{\delta}_f\})\\
&=-[M]\{I\}\ddot{u}_g+[G_s]\{\delta_f\}+[G_{sc}]\{\dot{\delta}_f\} \qquad (3)
\end{aligned}
$$

where

$[C_B]$: viscous boundary matrix for the base boundary.

$[C_s]$: viscous boundary matrix for the side boundary.

$[G_s]$: boundary stiffness matrix associated with the displacements of the free field.

$[G_{cs}]$: boundary damping matrix associated with the velocities of the free field

$\{\delta_B\}$: displacement vector of which components correspond to the components on the basal layer of the $\{\delta\}$.

$\{\delta_s\}$: displacement vector of which components correspond to the components on the side boundary of the $\{\delta\}$.

$\{\delta_f\}$: displacement vector of the free field

The 4th and 5th terms imply radiation to the basal layer and radiation to the side free field, respectively. The 2nd and 3rd terms in the righthand side of Eq.(3) are forces due to the motion of the free field.

In the present paper, $[C_B]$, $[C_s]$, $[G_s]$ and $[G_{cs}]$ are called "the boundary matrix" for convenience.

Displacements $\{\delta\}$ are obtained from the Eq.(3) and time history response is also obtained by means of well known Fourier transformation technique.

2.2 Formulation of the boundary matrices

2.2.1 Displacements and coordinates

Fig.2 shows the displacement and coordinate system of the analysis. Displacements

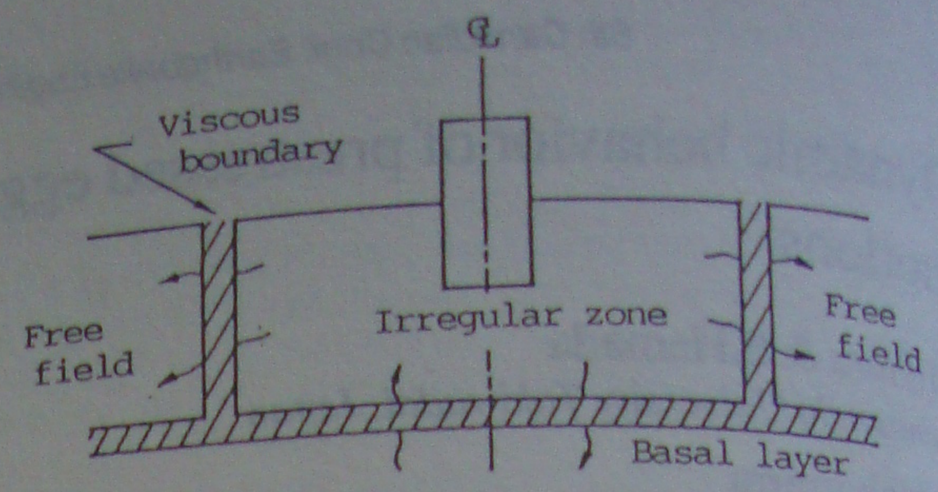

Fig.1 General view of soil-structure system analysed.

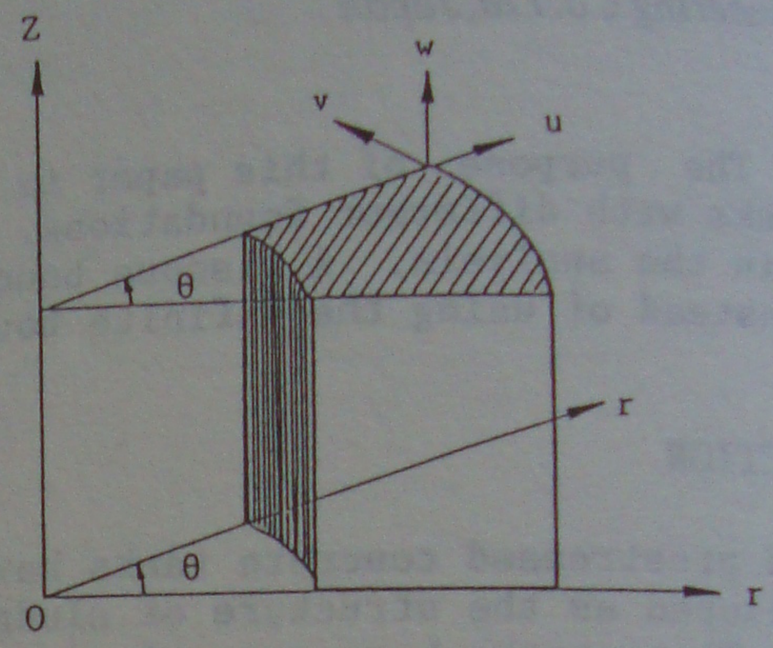

Fig.2 Coordinate system and displacement components.

u, v, and w are noted as the displacements in r, v and θ directions for the ring element. These displacements are represented in the form of Fourier series (Zienkiewicz, 1982(a)):

$$
\left.
\begin{aligned}
u &= \sum_{n=0}^{N} u_n \cos n\theta\\
v &= -\sum_{n=0}^{N} v_n \sin n\theta\\
w &= \sum_{n=0}^{N} w_n \cos n\theta
\end{aligned}
\right\} \qquad (4)
$$

where u_n, v_n and w_n are amplitudes of harmonic n. N is determined from the accuracy to be desired. For simplicity, notations u, v and w in this chapter means u_n, v_n and w_n, respectively.

2.2.2 Viscous boundary

The virtual work δW done on the boundary, which is the 3rd term of Eq.(1) is given as

$$\delta W = \int_S T_j \, \delta u_j \, ds \qquad (5)$$

$$T_j = \rho V \dot{u}_j \qquad (6)$$

where V is the velocity in the noted directions, that is, the transverse wave velocity Vs or the longitudinal wave velocity Vp. $\dot{u}$ is the relative velocity on the boundary.

2.2.3 Viscous boundary matrix for the base boundary $[C_B]$

The virtual work δW_b done on the base boundary can be represented in the following form

$$\delta W_b = \delta W_r + \delta W_\theta + \delta W_z \qquad (7)$$

These three parts can be obtained in the similar way. The wave velocity and relative velocity are Vs and $\dot{u}_g \cos n\theta$ in r-direction. The traction T_r in Eq.(6) is given by

$$T_r = \rho V_s \dot{u} \cos n\theta \qquad (8)$$

The virtual work δW_r done on the base between nodes j and j+1 is obtained by substituting Eq.(8) into Eq.(5) and by taking the virtual displacement as $\delta u \cos n\theta$ (see Fig.3). Assuming that displacement and the relative velocity are linear between nodes j and j+1, the virtual work δW_r is evaluated by

$$\delta W_r = \{ \delta u_j \;\; \delta u_{j+1} \} \frac{\pi \rho V_s \ell}{12} [R] \begin{Bmatrix} \dot{u}_j \\ \dot{u}_{j+1} \end{Bmatrix} \qquad (9)$$

where

$$[R] = \begin{bmatrix} 3r_j + r_{j+1} & r_j + r_{j+1} \\ r_j + r_{j+1} & r_j + 3r_{j+1} \end{bmatrix} \qquad (10)$$

Using the nodal force vector $\{f^r\} = \{f^r_j \; f^r_{j+1}\}^T$, the virtual work δW_r is also expressed as

$$\delta W_r = \{ \delta u_j \;\; \delta u_{j+1} \} \{ f^r \} \qquad (11)$$

Eqs.(9) and (11) produce the nodal force vector $\{f_r\}$ as

$$\begin{Bmatrix} f^r_j \\ f^r_{j+1} \end{Bmatrix} = \frac{\pi \rho V_s \ell}{12} [R] \begin{Bmatrix} \dot{u}_j \\ \dot{u}_{j+1} \end{Bmatrix} \qquad (12)$$

The Tractions T_θ and T_z in θ and z directions are given by

$$\left. \begin{aligned} T_\theta &= \rho V_s \dot{v} \sin n\theta \\ T_z &= \rho V_p \dot{w} \cos n\theta \end{aligned} \right\} \qquad (13)$$

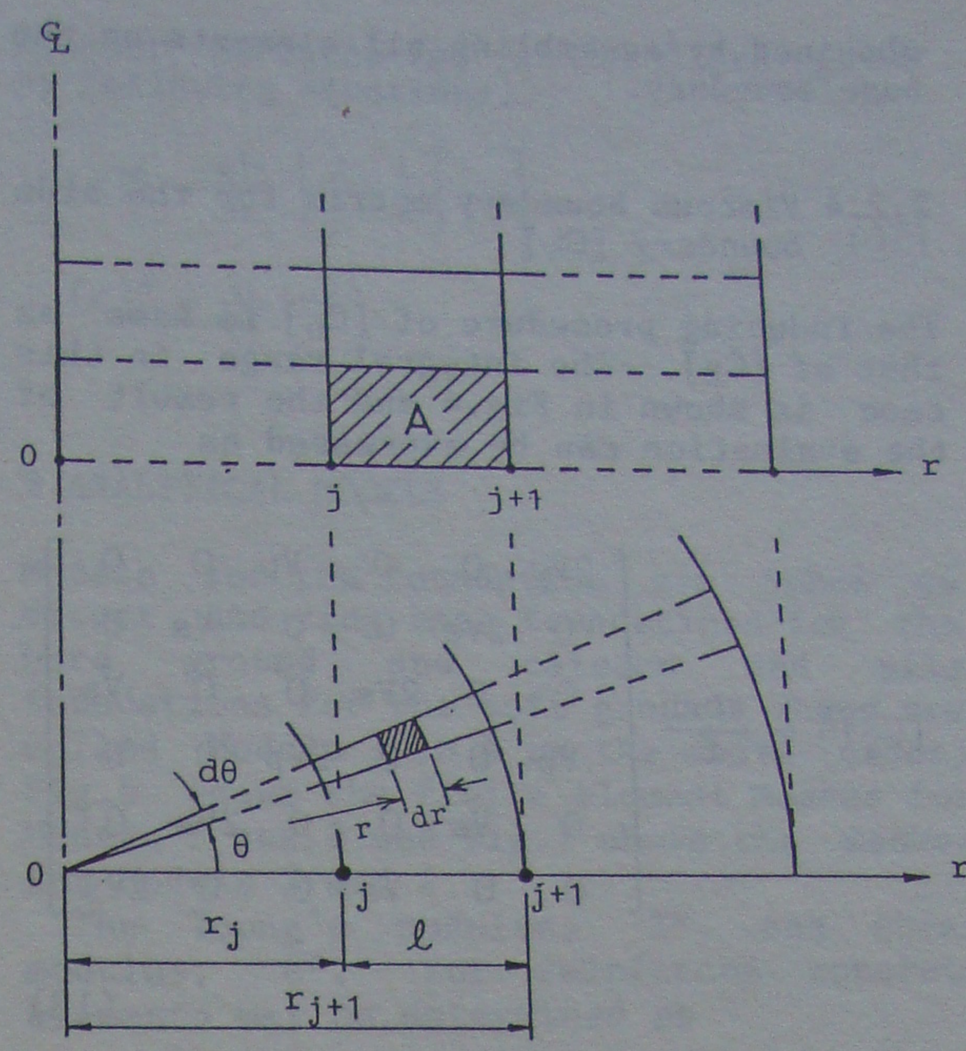

Fig.3 Notations for integration of the virtual work done on the base boundary.

Employing these tractions in the same way as r direction, a relationship between the nodal vector and the relative velocity vector is obtained as

$$\{ f \}^A = [C_B]^A \{ \dot{\delta} \}^A \qquad (14)$$

where

$$\left. \begin{aligned} \{f\}^A &= \{f^r_j \; f^\theta_j \; f^z_j \; f^r_{j+1} \; f^\theta_{j+1} \; f^z_{j+1}\}^T \\ \{\dot{\delta}\}^A &= \{\dot{u}_j \; \dot{v}_j \; \dot{w}_j \; \dot{u}_{j+1} \; \dot{v}_{j+1} \; \dot{w}_{j+1}\}^T \end{aligned} \right\} \qquad (15)$$

$$[C_B]^A = \frac{\pi \rho \ell}{12} \begin{bmatrix} \alpha V_s & 0 & 0 & \beta V_s & 0 & 0 \\ 0 & \alpha V_s & 0 & 0 & \beta V_s & 0 \\ 0 & 0 & \alpha V_p & 0 & 0 & \beta V_p \\ \beta V_s & 0 & 0 & \gamma V_s & 0 & 0 \\ 0 & \beta V_s & 0 & 0 & \gamma V_s & 0 \\ 0 & 0 & \beta V_p & 0 & 0 & \gamma V_p \end{bmatrix} \qquad (16)$$

$$\left. \begin{aligned} \alpha &= 3r_j + r_{j+1} \\ \beta &= r_j + r_{j+1} \\ \gamma &= r_j + 3r_{j+1} \end{aligned} \right\} \qquad (17)$$

The matrix $[C_B]^A$ in Eq.(14) is evaluated for the element A in the base boundary (see Fig.3), and the total matrix $[C_B]$ is

obtained by assembling all elements on the base boundary.

2.2.4 Viscous boundary matrix for the side boundary $[C_S]$

The inducing procedure of $[C_S]$ is same as that of $[C_B]$. The integral range in this case is shown in Fig.4 and the result of the evaluation can be expressed as

$$[C_S]^A = \frac{\pi\rho rh}{6}\begin{bmatrix} 2Vp & 0 & 0 & Vp & 0 & 0 \\ 0 & 2Vs & 0 & 0 & Vs & 0 \\ 0 & 0 & 2Vs & 0 & 0 & Vs \\ Vp & 0 & 0 & 2Vp & 0 & 0 \\ 0 & Vs & 0 & 0 & 2Vs & 0 \\ 0 & 0 & Vs & 0 & 0 & 2Vs \end{bmatrix} \tag{18}$$

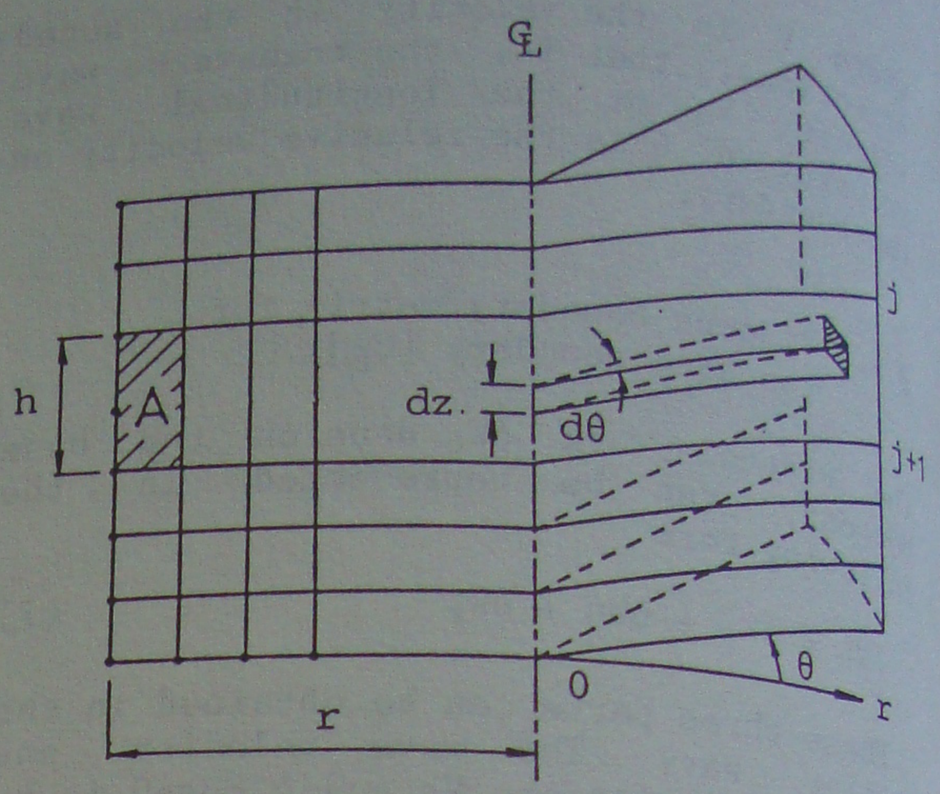

Fig.4 Notations for integration of the virtual work done on the side boundary.

2.2.5 Side boundary stiffness matrix $[G_S]$

Stresses of three dimensional body produced between the vertical boundary surface and the free field surface are σ_r, $\tau_{r\theta}$ and τ_{zr} as shown in Fig.5. The virtual work is obtained from multiplying the resultant forces produced by these stresses by the corresponding deformations.

For the shear vibration, that is, horizontal vibration, the amplitude of horizontal displacement u_f, becomes a function of z. Only the stress, τ_{zr}, exists on the side boundary surface in this case and is determined as

$$\tau_{zr} = \mu\gamma_{zr} = \mu\frac{\partial u_f}{\partial z}\cos n\theta \tag{19}$$

where μ is the shear modulus.

The virtual work done on this surface is given by

$$\delta W = \int_0^h \int_0^{2\pi} \tau_{zr}\,\delta u_f \cos n\theta\, r\,d\theta dz \tag{20}$$

Assuming that the displacement of free field u_f is linear between the nodes j and j+1, the virtual work δW is expressed as

$$\delta W = \{\delta u_{f,j}\ \delta u_{f,j+1}\}\frac{\pi\mu r}{2}\begin{bmatrix} -1 & 1 \\ -1 & 1 \end{bmatrix}\begin{Bmatrix} u_{f,j} \\ u_{f,j+1} \end{Bmatrix} \tag{21}$$

The nodal forces are also expressed as

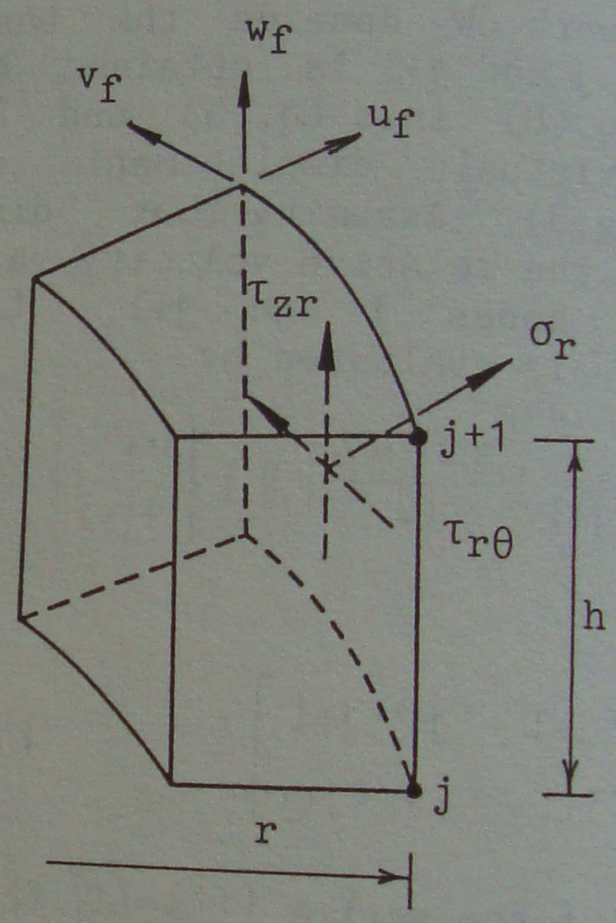

Fig.5 Stress components produced on the side boundary.

$$\begin{Bmatrix} f^z_{f,j} \\ f^z_{f,j+1} \end{Bmatrix} = \frac{\pi\mu r}{2}\begin{bmatrix} -1 & 1 \\ -1 & 1 \end{bmatrix}\begin{Bmatrix} u_{f,j} \\ u_{f,j+1} \end{Bmatrix} \tag{22}$$

Similarly nodal forces due to the vertical vibration results in

$$\begin{Bmatrix} f^r_{f,j} \\ f^r_{f,j+1} \end{Bmatrix} = \frac{\pi\lambda r}{2}\begin{bmatrix} -1 & 1 \\ -1 & 1 \end{bmatrix}\begin{Bmatrix} w_{f,j} \\ w_{f,j+1} \end{Bmatrix} \tag{23}$$

Eqs.(22) and (23) are summarized in the matrix form

$$\{f_f\}^A = [G_s]^A\{\delta_f\}^A \tag{24}$$

where

$$\{f_f\}^A=\{f^r_{f,j}\ f^\theta_{f,j}\ f^z_{f,j}\ f^r_{f,j+1}\ f^\theta_{f,j+1}\ f^z_{f,j+1}\}$$

$$\{\delta_f\}^A=\{u_{f,j}\ v_{f,j}\ w_{f,j}\ u_{f,j+1}\ v_{f,j+1}\ w_{f,j+1}\} \qquad (25)$$

$$[G_S]^A=\frac{\pi r}{2}\begin{bmatrix} 0 & 0 & -\lambda & 0 & 0 & \lambda \\ 0 & 0 & 0 & 0 & 0 & 0 \\ -\mu & 0 & 0 & \mu & 0 & 0 \\ 0 & 0 & -\lambda & 0 & 0 & \lambda \\ 0 & 0 & 0 & 0 & 0 & 0 \\ -\mu & 0 & 0 & \mu & 0 & 0 \end{bmatrix} \qquad (26)$$

The total matrix for side boundary, $[G_S]$, can be obtained by assembling the individual boundary matrix $[G_S]^A$ on the side boundary.

2.3 Damping matrix [C] and boundary damping matrix $[G_{CS}]$

The damping matrix [C] and boundary damping matrix $[G_{CS}]$ are given by assuming Rayleigh's damping as following :

$$[C]=\frac{h}{\pi f}[K],\quad [G_{CS}]=\frac{h}{\pi f}[G_S] \qquad (27)$$

where h is the damping factor for a frequency of f which is commonly taken as the natural frequency of surface ground.

2.4 Free field ground motion

The equation of motion for free field is briefly given as

$$[K]^f\{\delta_f\}+[C]^f\{\dot{\delta}_f\}+[M]^f\{\ddot{\delta}_f\}=-[M]^f\{I\}\ddot{u}_g \qquad (28)$$

where, {I} is the unit vector and the matrices $[K]^f$, $[C]^f$, $[M]^f$ are constructed by adding the submatrices $[k]^A$, $[c]^A$, $[m]^A$. $[k]^A$ depends on the input direction as follows.

(i) Horizontal excitation

$$[k]^A=\frac{\mu}{h}\begin{bmatrix} 1 & -1 \\ -1 & 1 \end{bmatrix} \qquad (29)$$

(ii) Vertical excitation

$$[k]^A=\frac{\lambda+2\mu}{h}\begin{bmatrix} 1 & -1 \\ -1 & 1 \end{bmatrix} \qquad (30)$$

Element matrices $[m]^A$ and $[c]^A$ are given by following equations.

$$\left.\begin{aligned}[m]^A&=\frac{\rho h}{6}\begin{bmatrix} 2 & 1 \\ 1 & 2 \end{bmatrix}\\ [c]^A&=\frac{h}{\pi f}[k]^A\end{aligned}\right\} \qquad (31)$$

3 ANALYTICAL MODELS

Models for the foundation are taken as direct and ring base foundations for the hard ground and caisson and pile foundations for the soft ground. These are called Models 1 to 4 as the above order. Fig.6 shows the finite element meshes for Models 1 and 2 and Fig.7 shows the meshes for Models 3 and 4.

The Young's modulus, E*, and shear modulus, G*, for reinforced concrete elements may be determined as

$$\left.\begin{aligned}E^*&=Ar\ Er+Ac\ Ec\\ G^*&=Ar\ Gr+Ac\ Gc\end{aligned}\right\} \qquad (32)$$

where A, E and G are the area per unit area, Young's Modulus and shear modulus, respectively. Subscripts r and c indicate reinforcing steel and concrete, respectively. These definition implies a relation of Ar+Ac=1.

The moduli of ring elements for the pile region are determined so as to be equivalent to these for mixed materials of piles and soil constructed in circle configurations. The equivalent Young's modulus, E_θ, in the angular direction is obtained as

$$E_\theta=\frac{E_pE_gA_pA_g}{E_pA_p+E_gA_g} \qquad (33)$$

where the subscripts p and g mean the pile and soil, respectively. The shear modulus in the angular direction is similarly determined. Young's moduli and shear moduli for the radius and vertical directions can be determined from Eq.(32), where the subscripts r and c are to be alternated to p and g. The constitutive matrix of the stiffness matrix for a anisotropic material is given in several publications (for example, Zienkiewicz, 1982(b)).

Interaction effect between the liquid container and tank wall is neglected in the present analysis. The mass of the liquid is treated as the virtual mass of the tank wall. This assumption is based on

the research done by Kotsubo(1985), which indicates that more than 93 percent of liquid container acts as the virtual mass.

Table 1 gives Young's and shear moduli for steel and concrete employed in the present analysis.

Table 1. Material constants.

	E (kg/cm^2)	G (kg/cm^2)
Steel	2.1×10^6	8.1×10^5
Concrete	1.4×10^5	6.3×10^4

4 ANALYTICAL RESULTS

In the analysis, deconvoluted El Centro 1940 NS component of the seismic wave was applied at the base to each model. Since this seismic wave has the maximum acceleration of 340 gal which is obtained from the measurement at the ground surface, and the maximum amplitude and frequency characteristics need not to be amended. The acceleration responses at the top of each model (A in Figs.6 and 7) are shown in Fig.8, and the displacement responses are shown in Fig.9. These are time histories in the radius direction (r-component).

The results of Models 1 and 2 represent similar behavior, whereas there is a difference in the maximum acceleration and displacement. The maximum acceleration of Model 1 is 600 gal and is 40 percent greater than that of Model 2. Similarly, the maximum displacement of Model 1 is 3.1 cm and is two times as large as that of Model 2. This implies that the ring concrete reduces accelerations and displacements.

Models 3 and 4 have caisson and pile foundations, respectively. High frequencies are distinguished in time histories of acceleration of both Models 3 and 4. These responses exhibit a pulse shape. The maximum acceleration of Model 3 is evaluated as 850 gal and is 15 percent less than that of Model 4. On the contrary, the maximum displacements of Models 3 and 4 are 1.2 cm and 0.73 cm, respectively. There is, however, no distinguished responses between these two models.

Figs. 10 and 11 show that distributions of the maximum principal stress, σ_1, and the maximum shearing stress, τ max. Notations B, C and D on the vertical line represent the locations of the tank in Figs. 6 and 7. G.L. and L.B. means the ground level and the boundary between the

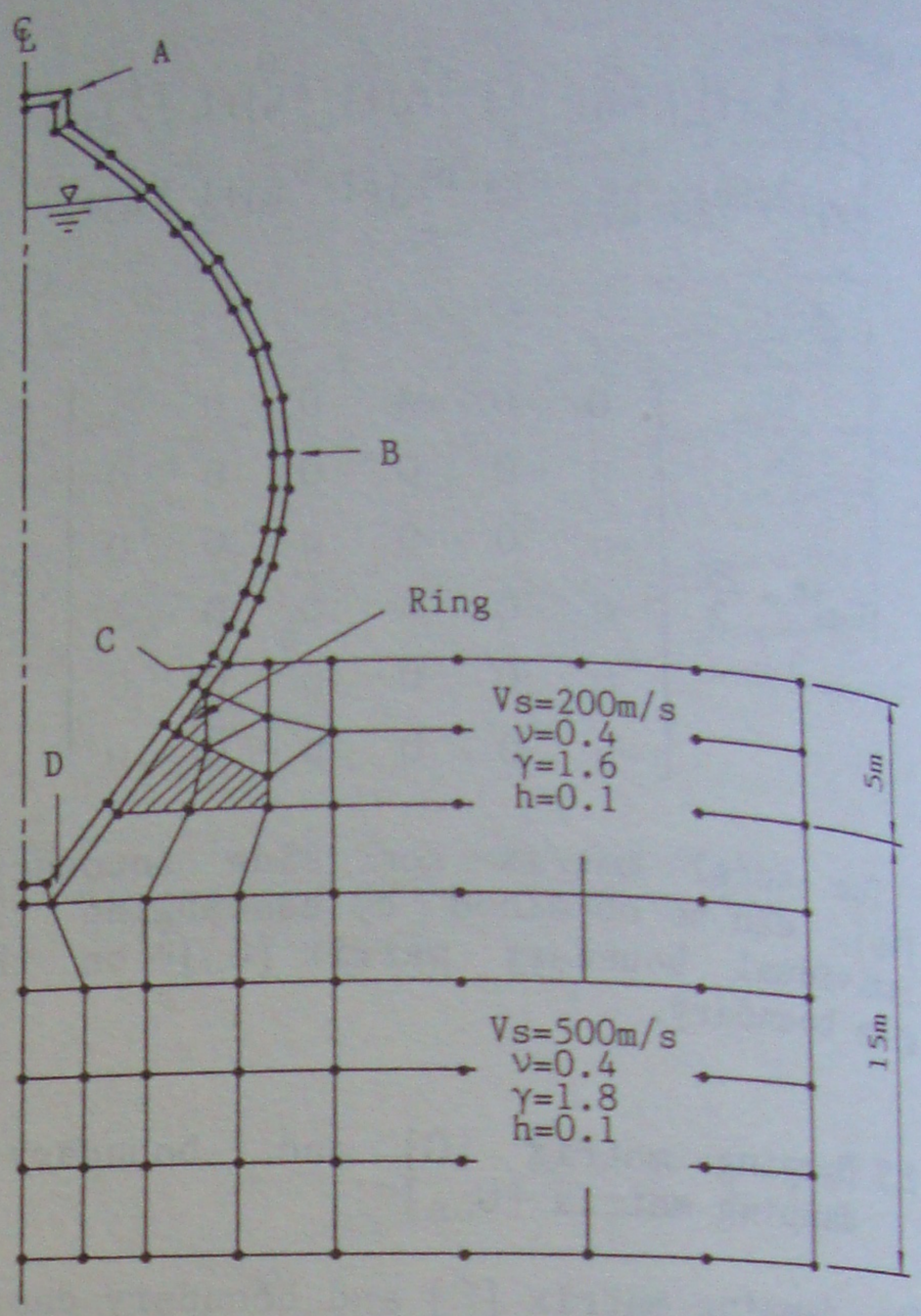

Fig.6 Finite element mesh for Model 1,2.

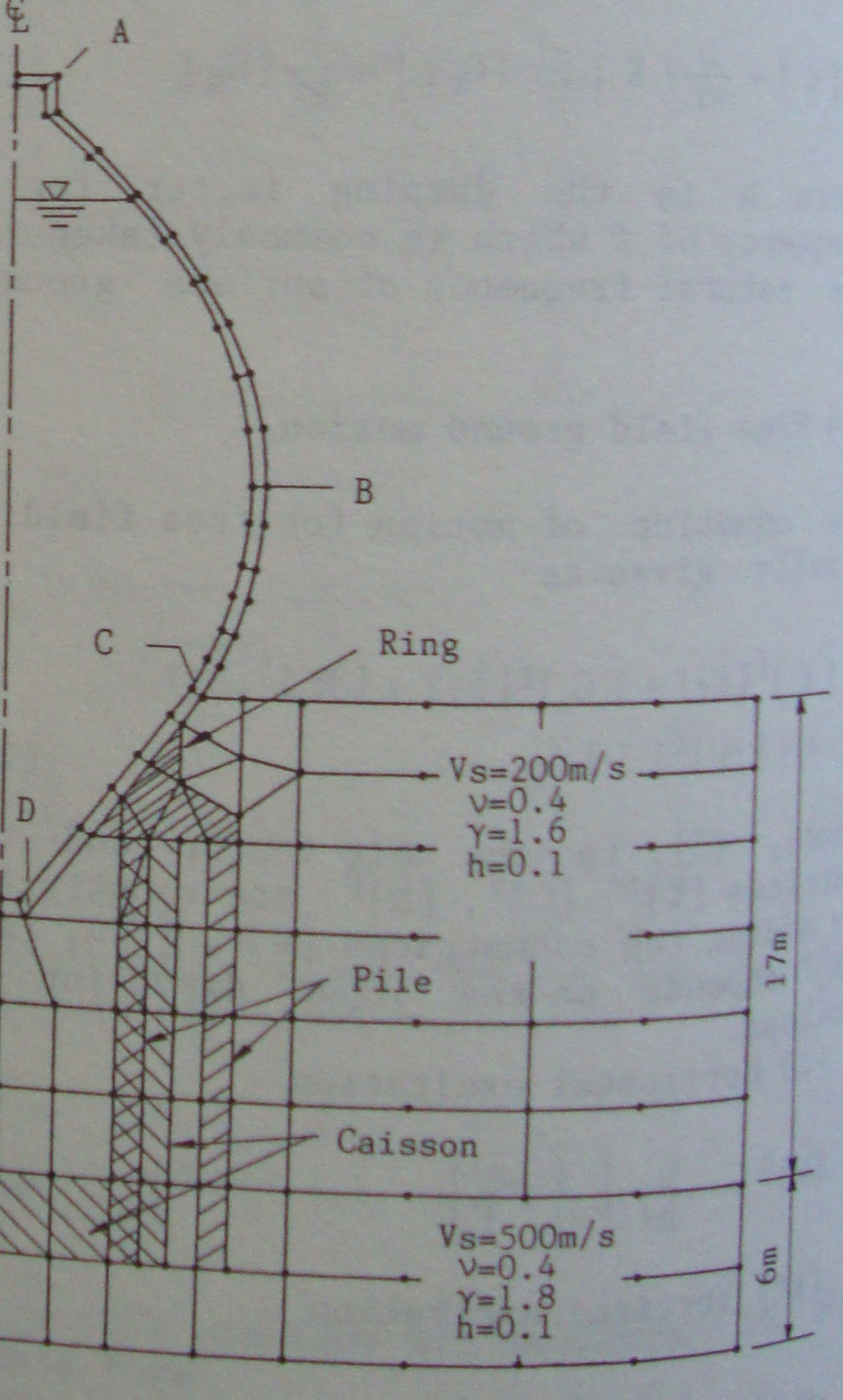

Fig.7 Finite element mesh for Model 3,4.

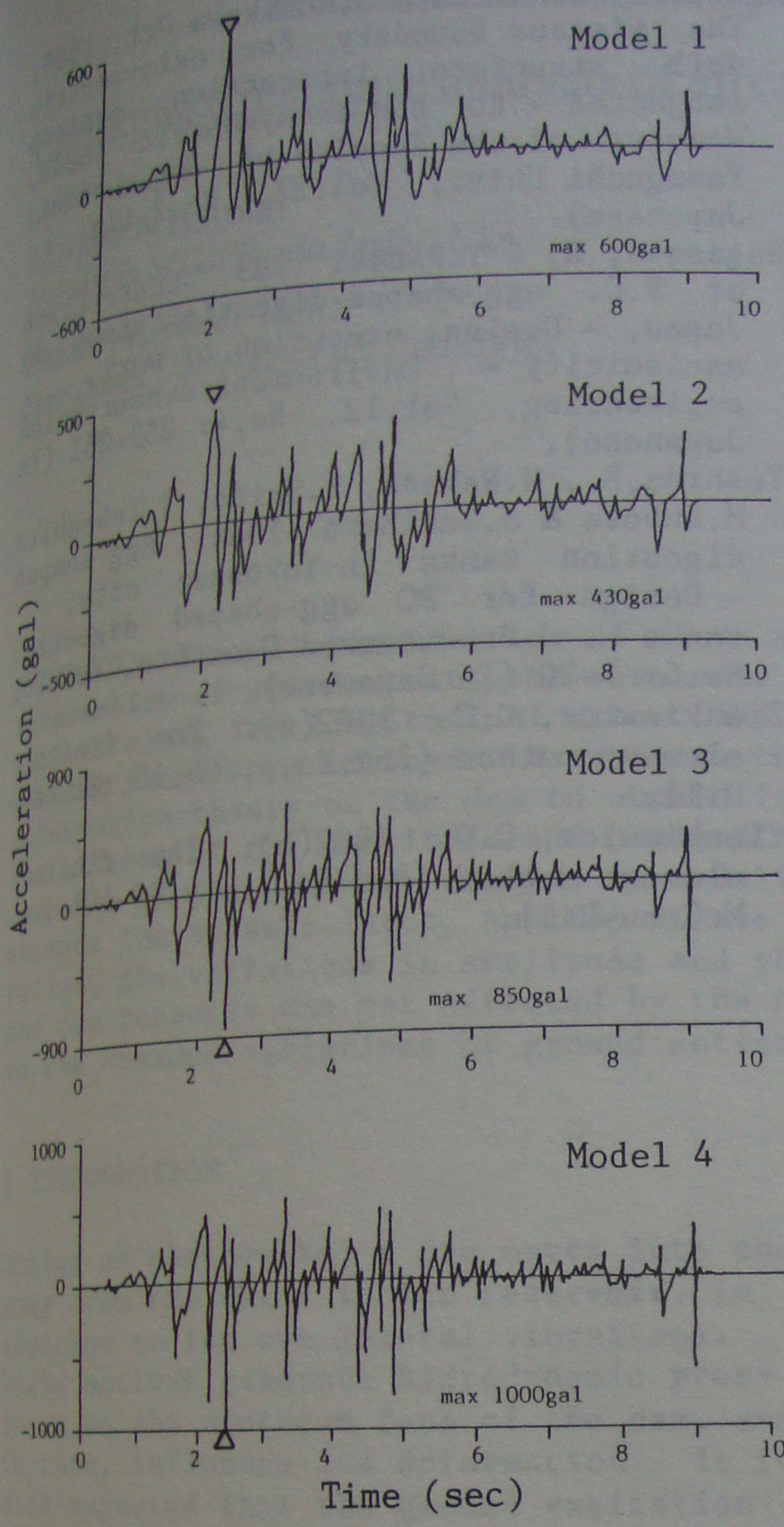

Fig.8 Time histories of acceleration.

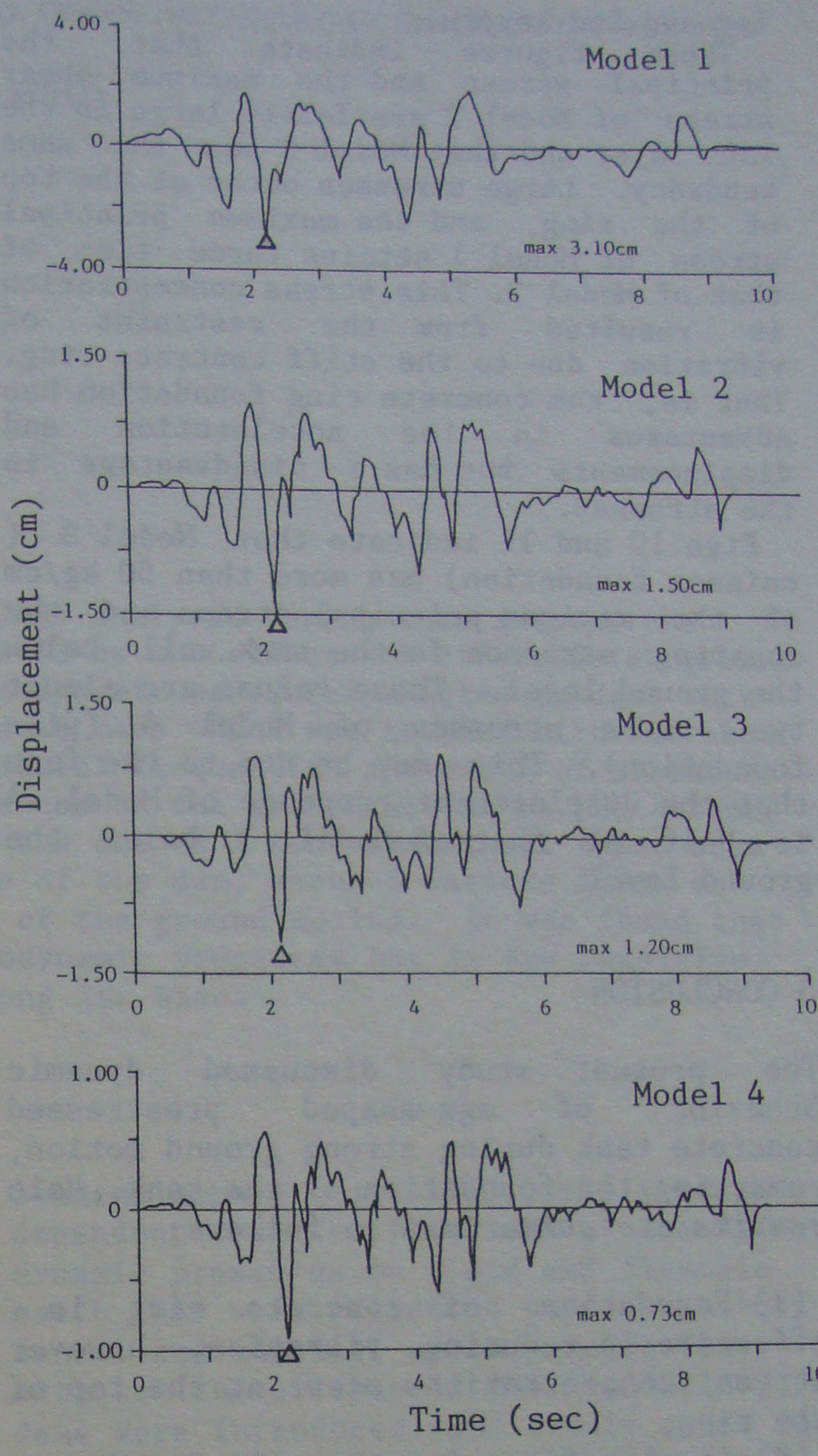

Fig.9 Time histories of displacement.

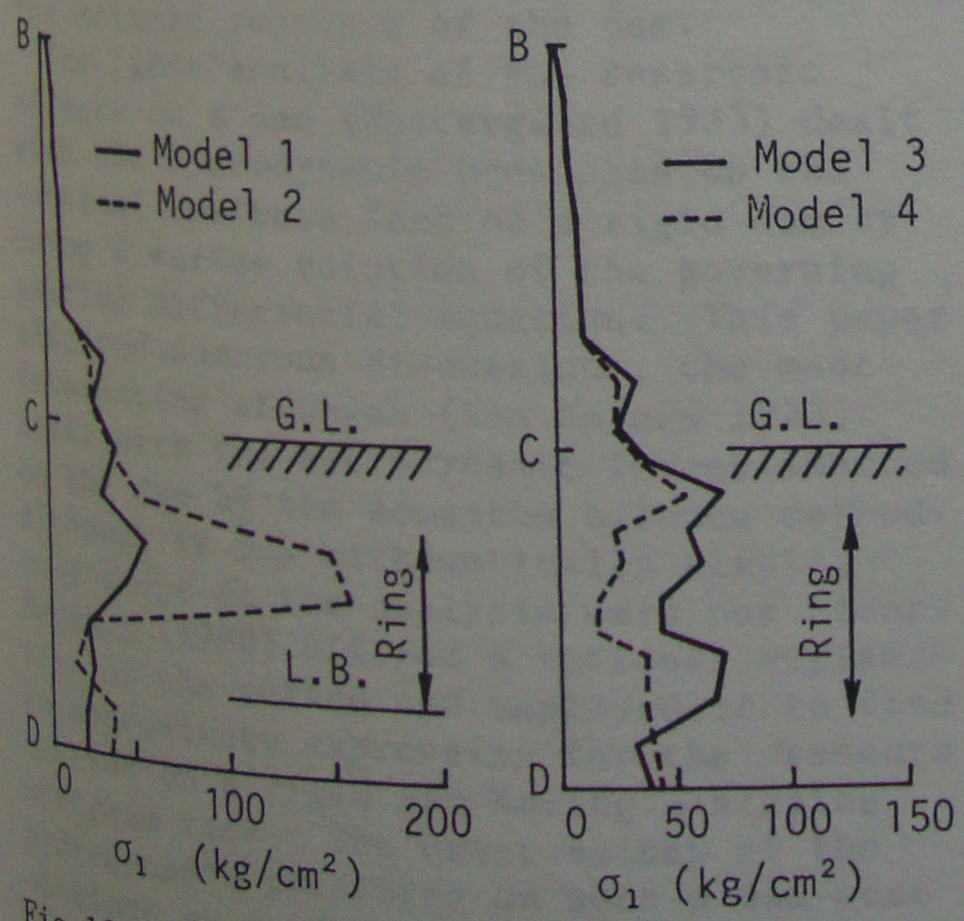

Fig.10 Distributions of the principal stress.

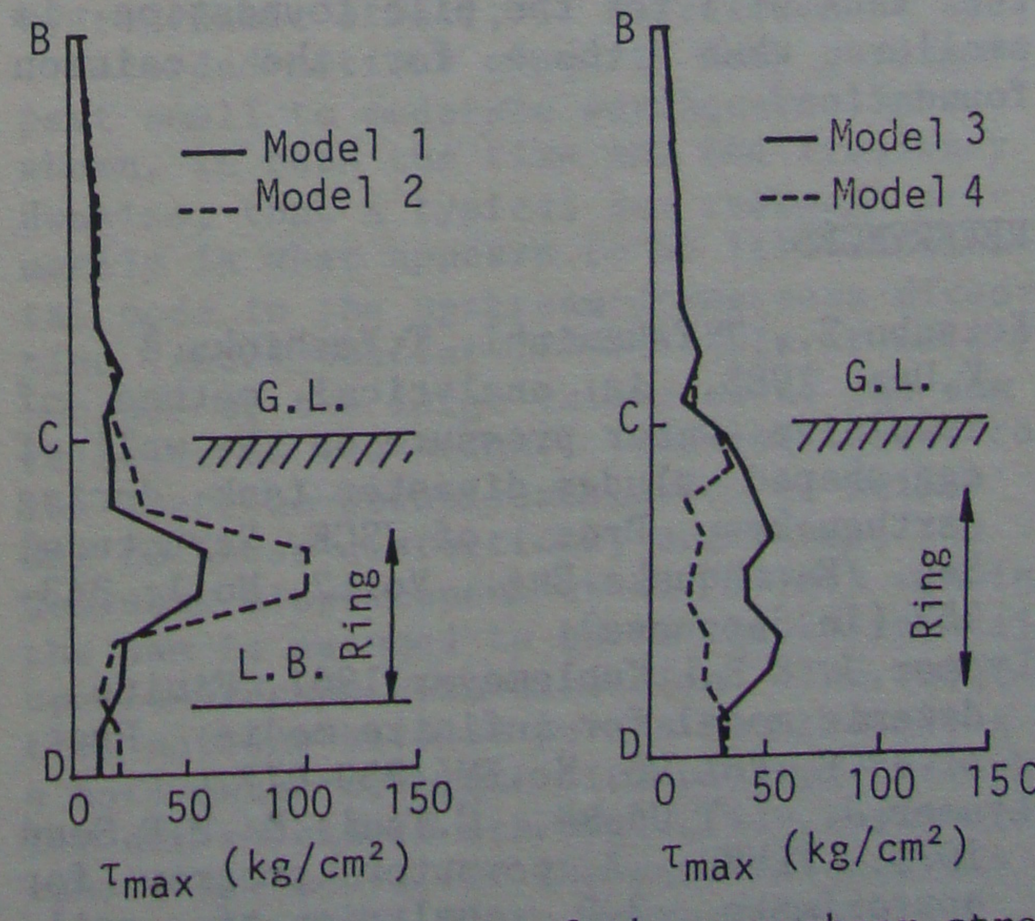

Fig.11 Distributions of the max.shear stress.

1st and 2nd layers.

These figures indicate that the principal stress and the maximum shear stress of Model 2 are fairly large in the 1st layer and that Model 1 has the same tendency. Large stresses occur at the top of the ring, and the maximum principal stress of Model 1 attains three time of that of Model 2. This stress concentration is resulted from the restraint of vibration due to the stiff concrete ring. That is, the concrete ring foundation has advantages in the acceleration and displacements but has a disadvantage in the stresses.

Figs.10 and 11 indicate that Model 3 (caisson foundation) has more than 50 kg/cm^2 of the maximum principal stress and the shearing stresses in the tank wall below the ground level. These values are almost two times stresses of Model 4 (pile foundation). This may be due to the fact that the displacement response of Model 4 is half of that of Model 3 below the ground level.

5 CONCLUSION

The present study discussed dynamic behavior of egg-shaped prestressed concrete tank during strong ground motion, remarking the foundation of the tank. Main results are summarized as follows;

(1) Foundation of concrete ring is effective in reducing vibration, however stress concentrations occur at the top of the ring.

(2) Accelerations for the pile foundation is larger than those for the caisson foundation. On the contrary, stresses in the tank wall for the pile foundation is smaller than those for the caisson foundation.

REFERENCES

Kotsubo,S., T.Takanishi, T.Yoshioka & K.Uno 1985. An analytical method of impulsive water pressure on the wall of egg-shaped sludge digester tank during earthquakes. Proc. of JSCE, Structural Eng. /Earthquake Eng., Vol.2, No.1: 343-352 (In Japanese).

Lysmer,J. & R.L.Kuhlemeyer 1967. Finite dynamic model for infinite media. Proc. of ASCE, Vol.95, No.EM4:859-877.

Lysmer,J., T.Udaka, C.Tsai & H.B.Seed 1975. FLUSH, A computer program for approximate 3-D analysis of soil-structure interaction problems. EERC 75-30.

Miura,F., S.Hamada & S.Morikawa Oct.,1986. The viscous boundary for axisymmetric soil structure interaction systems subjected to non-axisymmetric loads. Memoirs of the faculty of Engineering, Yamaguchi Univ., Vol.37, No.2 (in Japanese).

Nagasawa, H. & T.Risaki 1983. Construction of P.C. egg-shaped digestion tanks in Japan, - Design, execution of work, aseismicity - . Environment conservation engineering, Vol.12, No.4: 253-261 (In Japanese).

Yoshida,S., H.Nakada, K.Saito, T.Takeshita, M.Kubota & S.Ishihara 1984. Egg-shaped digestion tanks in Yokohama city, - Design for PC egg-shaped digestion tanks -. J.Prestressed Concrete, Vol.26, No.5: 7-20 (In Japanese).

Zienkiewicz, O.C. 1982(a). The finite element method (3rd Ed.), Ch.15 :McGraw-Hill.

Zienkiewicz, O.C. 1982(b). The finite element method (3rd Ed.), p.99-101 : McGraw-Hill.